11th AIAA/CEAS Aeroacoustics Conference (26th AIAA Aeroacoustics Conference)
23 - 25 May 2005, Monterey, California

AIAA 2005-2817

Noise Radiated by a High-Reynolds-number 3-D Airfoil

Olivier Marsden[*], Christophe Bogey[†], Christophe Bailly[‡]

Laboratoire de Mécanique des Fluides et d'Acoustique

Ecole Centrale de Lyon & UMR CNRS 5509

69134 Ecully, France.

A large-eddy simulation (LES) of the flow around a NACA0012 airfoil at a chord-based Reynolds number of 5.0×10^6 and a Mach number of 0.22 is performed, and its results are compared with experimental data. The airfoil is placed without incidence to the turbulence-free incoming flow. The boundary layer in this configuration is expected to be initially laminar, and to transition to a turbulent state along the second half of the airfoil chord, and as such constitutes a challenging test-case for LES computations to reproduce. The LES calculation is performed with a parallel code resolving the full compressible Navier-Stokes equations on structured curvilinear grids with optimized explicit high-order finite-difference schemes and filters. A preliminary two-dimensional simulation and a full three-dimensional simulation are performed for the same airfoil configuration. The two-dimensional simulation shows substantial discrepancies with available experimental data. On the other hand, flow results from the three-dimensional simulation compare favorably, and the LES is shown to capture boundary layer dynamics reasonably well. These results are a first step towards the development of the direct computation of noise emitted by a high-Reynolds-number airfoil.

I. Introduction

Over the past ten years, large eddy simulations have been shown to succeed in calculating increasingly complex flows, up to the point where LES is becoming a useful tool for industrial design processes. However, lifting devices such as airfoils are still computationally challenging, due to the occurrence of complex flow behaviours such as laminar to turbulent transition and boundary layer separation. Furthermore, capturing the unsteady flow sufficiently precisely to preserve the radiated noise is harder still, and consequently to date most attempts at calculating the noise radiated by a three-dimensional lifting device have resorted to an acoustic analogy to obtain the acoustic far field. The direct computation of the noise radiated by airfoils remains an interesting goal. Indeed it can not only provide a reference useful for improving less computationally demanding prediction methods, but can also help to shed some light on noise generation processes.

The demands on the accuracy of the numerical approach used to perform a direct noise computation, as well as on its capacity to cope with a small number of points per wavelength, are particularly stringent, because of the many orders of magnitude separating acoustic energies and wavelengths from their flow counterparts. Both explicit schemes, such as Tam and Webb's DRP scheme[1] or those proposed more recently by Bogey and Bailly,[2] and implicit ones such as Lele's Padé-type schemes,[3,4] have been shown to meet the above criteria and have been successfully applied to direct aeroacoustic simulations. High-order schemes typically require large stencils, and are therefore generally implemented on structured grids. Complex curved geometries, while relatively easy to treat thanks to unstructured methods, are often impossible to mesh with a structured cartesian grid without resorting to extrapolation techniques[5] and their associated problems for the implementation of solid boundary conditions. This difficulty can be overcome by the use of curvilinear

*Ph.D Student
†CNRS Research Scientist
‡Professor

transformations combined with overset multiple grid techniques, often referred to as chimera techniques.[6] Such methods have sparked considerable interest over the last few years, and recent simulations have shown the feasibility of multiple grid high-fidelity simulations, in the fields of fluid mechanics and electromagnetics, and also more specifically in that of aeroacoustics, for example by Delfs *et al.* who used such methods to examine interactions between a vortex and an airfoil trailing edge.[7]

Airfoil trailing-edge noise has been the subject of much research, from a theoretical point of view as well as both experimentally and numerically. Many theoretical models have been proposed, often based on Lighthill's analogy.[8–11] Experimentally, various methods have been employed to measure trailing-edge noise and to separate it from extraneous noise sources: Schlinker[12] used a directional microphone to study the TE noise resulting from an airfoil with untripped boundary layers at zero angle of attack, while Yu and Yoshi[13] and Brooks and Hodgson[14] identified TE noise thanks to cross-correlation analyses.

The computational study of airfoil trailing-edge noise is more recent than its analytical and experimental counterparts. Singer *et al.*[15] generated for instance vortices just upstream of the trailing edge of an airfoil in an inviscid flow, and used the resulting unsteady CFD data as an input to the FW-H equation to obtain the acoustic field. Lummer *et al.*[7] examined the radiation emitted by individual vortices crossing a sharp trailing edge, by resolving both linear and non-linear disturbance equations around a Joukowski airfoil. Wang and Moin[16] performed an LES around an asymmetrically beveled trailing edge and applied an integral form of the Lighthill equation to obtain the far acoustic field. Manoha *et al.*[17] used the Linearized Euler Equations and a three-dimensional Kirchhoff formulation to propagate near-field data resulting from an LES around a NACA0012 airfoil at $5°$ incidence and at a chord-based Reynolds number of 2.86×10^6.

Direct noise computations have the advantage, with respect to the hybrid methods presented above, of yielding all relevant flow and acoustic quantities in a single computation. Furthermore they have the potential to alleviate many of the difficulties inherent to experimental trailing-edge studies. The effect of the upstream turbulence level, for example, is considerably easier to study numerically than experimentally, as is the effect of wind-tunnel geometry on boundary layer development and thus on radiated noise.

In the present work, a three-dimensional parallel simulation code resolving the curvilinear compressible Navier-Stokes equations on structured grids with high-order optimized finite difference schemes and explicit filters, is used to study the flow around a NACA0012 airfoil, with the aim of performing a direct noise computation. The airfoil is placed at zero incidence to the uniform upstream flow, and has a chord-based Reynolds number of 500,000. In these conditions, the boundary layer is expected to transition from an initially laminar state to a turbulent state a little upstream from the trailing edge of the airfoil.[18] Consequently, the boundary layers crossing the trailing edge are turbulent, and trailing-edge noise is thus generated. This constitues a difficult test-case for the LES solver, since the transition to turbulence in the boundary layer is expected to be very sensitive to parameters such as numerical accuracy, grid discretization and sub-grid-scale treatment.

The paper is presented as follows. After a brief description of the curvilinear equations, numerical aspects including the numerical algorithm, boundary conditions and parallelization are detailed. A preliminary two-dimensional direct simulation of the flow and acoustic field around a NACA0012 airfoil at a Reynolds number of 500,000 and a Mach number of 0.22 is then presented. Its flow results are shown to differ substantially from experimental data. Finally we describe a three-dimensional LES of the same airfoil configuration. Mean flow values and boundary-layer transition locations are shown to compare favorably with experimental data.

II. Curvilinear equations

High-order LES simulations having proven their value in the study of noise-generation mechanisms in unbounded flows, we are developing similar methods for more complex curvilinear geometries.

The full Navier-Stokes equations are solved on a computational grid which is obtained from the body-fitted grid by applying a suitable curvilinear coordinate transformation. The three-dimensional transformed equations can be written

$$\begin{aligned}\frac{\partial}{\partial t}\left(\frac{\mathbf{U}}{J}\right) &+ \frac{\partial}{\partial \xi}\left\{\frac{1}{J}\left[\xi_x(\mathbf{E_e}-\mathbf{E_v}+\mathbf{q_x})+\xi_y(\mathbf{F_e}-\mathbf{F_v}+\mathbf{q_y})+\xi_z(\mathbf{G_e}-\mathbf{G_v}+\mathbf{q_z})\right]\right\}\\ &+ \frac{\partial}{\partial \eta}\left\{\frac{1}{J}\left[\eta_x(\mathbf{E_e}-\mathbf{E_v}+\mathbf{q_x})+\eta_y(\mathbf{F_e}-\mathbf{F_v}+\mathbf{q_y})+\eta_z(\mathbf{G_e}-\mathbf{G_v}+\mathbf{q_z})\right]\right\}\\ &+ \frac{\partial}{\partial \zeta}\left\{\frac{1}{J}\left[\zeta_x(\mathbf{E_e}-\mathbf{E_v}+\mathbf{q_x})+\zeta_y(\mathbf{F_e}-\mathbf{F_v}+\mathbf{q_y})+\zeta_z(\mathbf{G_e}-\mathbf{G_v}+\mathbf{q_z})\right]\right\} = 0\end{aligned}$$

where $\mathbf{U} = (\rho, \rho u, \rho v, \rho w, \rho e_t)^T$, $J = |\partial(\xi,\eta,\zeta)/\partial(x,y,z)|$ is the Jacobian of the geometric transformation between the physical space (x,y,z) and the computational space (ξ,η,ζ), $\mathbf{E_e}, \mathbf{F_e}$ and $\mathbf{G_e}$ are the inviscid fluxes and $\mathbf{E_v}$, $\mathbf{F_v}$ and $\mathbf{G_v}$ the viscous ones, given by the following classical expressions

$$\mathbf{E_e} = \begin{pmatrix} \rho u \\ \rho u^2 + p \\ \rho u v \\ \rho u w \\ (\rho e_t + p) u \end{pmatrix} \quad \mathbf{E_v} = \begin{pmatrix} 0 \\ \tau_{xx} \\ \tau_{xy} \\ \tau_{xz} \\ u\tau_{xx} + v\tau_{xy} + w\tau_{xz} \end{pmatrix}$$

$$\mathbf{F_e} = \begin{pmatrix} \rho v \\ \rho u v \\ \rho v^2 + p \\ \rho v w \\ (\rho e_t + p) v \end{pmatrix} \quad \mathbf{F_v} = \begin{pmatrix} 0 \\ \tau_{xy} \\ \tau_{yy} \\ \tau_{yz} \\ u\tau_{xy} + v\tau_{yy} + w\tau_{yz} \end{pmatrix}$$

$$\mathbf{G_e} = \begin{pmatrix} \rho w \\ \rho u w \\ \rho v w \\ \rho w^2 + p \\ (\rho e_t + p) w \end{pmatrix} \quad \mathbf{G_v} = \begin{pmatrix} 0 \\ \tau_{xz} \\ \tau_{yz} \\ \tau_{zz} \\ u\tau_{xz} + v\tau_{yz} + w\tau_{zz} \end{pmatrix}$$

In the above equations, ρ refers to the fluid density, u, v and w refer to the velocity components in the x, y and z directions, and p to the pressure. Taking into account the perfect gas law, the total energy e_t is given by $e_t = p/[(\gamma-1)\rho] + (u^2+v^2+w^2)/2$. The heat term $\mathbf{q}$ is given by Fourier's law, and the components of the stress tensor $\boldsymbol{\tau}$ are those of a viscous Newtonian fluid.

III. Numerical aspects

A. Numerical algorithm and boundary conditions

A 2-D structured body-fitted grid is created around the NACA0012 airfoil. For the three-dimensional simulations, this grid is duplicated in the spanwise direction with a constant δz spacing. The use of structured highly regular grids is in general appropriate for high-order finite-difference schemes. In this work, eleven-point finite-difference schemes are used to calculate spatial derivatives over the entire computational domain, including solid-wall boundary zones. Over the interior part of the computational grid, a centered optimized scheme[2] is used. This scheme is dissipation-free thanks to its centered nature, and generates only very low dispersion for waves discretized by at least four points per wavelength, and is thus ideally suited to the direct computation of the sound field radiated by turbulent flows. Non-physical high-frequency oscillations, resulting from the use of centered high-order schemes on non-uniform grids and from solid-wall boundary conditions, are removed by an explicit optimized eleven-point filter.[2] Near solid boundaries, the centered high-order eleven-point scheme and filter cannot be used. It is possible to use centered schemes up to the solid wall, but at the cost of reducing the stencil size and order of the schemes and filters, and thus deteriorating the overall numerical precision near the wall. Instead of this approach, non-centered eleven-point optimized schemes developed specifically for boundary treatment[19] are used for spatial derivatives, together with the corresponding non-centered optimized filters. A good illustration of the benefits of using non-centered optimized schemes and filters near solid walls is given by Visbal and Gaitonde.[20] The association of high-order non-centered schemes and filters near the solid wall makes it possible to maintain high numerical accuracy, both in terms of dispersion and in terms of dissipation, while employing small numbers of points per wavelength that would yield poor results if lower-order centered schemes and filters were used. The same centered and non-centered schemes are used to calculate the partial derivatives $\partial(\xi,\eta,\zeta)/\partial(x,y,z)$ of the grid transformation's Jacobian matrix, thanks to the expression

$$J = \frac{1}{|J^{-1}|}\left[\text{cofactors}(J^{-1})\right]^T$$

A no-slip wall condition is imposed at the airfoil's surface, and three-dimensional far-field radiation conditions developed by Bogey and Bailly[21] are used. A periodic condition is imposed in the spanwise direction. The simulation domain extends only one half of an airfoil chord downstream from the trailing edge for reasons of computational cost, and therfore a sponge zone in the last 20 points of the wake region is implemented to dampen vortical structures before they reach the outgoing boundary condition. Explicit time integration is performed with a six-stage Runge-Kutta scheme optimized for angular frequencies up to $\omega\Delta t = \pi/2$, implemented in a low-storage form.
The simulation code has been tested on numerous two-dimensional test-cases, including a two-body acoustic scattering problem[22] and a low-Reynolds-number flow around a cylinder. Results[23] were shown to be in good agreement with the corresponding analytical solutions and experimental data.
In the LES approach presented here, filtering plays a dual role. It is used not only to remove spurious high-frequency (typically grid-to-grid) oscillations which are generated close to geometrical singularities, but also as an implicit form of subgrid-scale treatment.[24] The spectral-like resolution of the high-order optimized filters leaves flow features larger than the filter cut-off wavelength unaffected, while cleanly removing energy being transferred to smaller wavelengths. Examples of LES performed with this technique, as well as more in-depth discussions on the role of the filtering, can be found in Bogey & Bailly.[25,26]

B. Parallelization

The code used for the three-dimensional simulations was parallelized using the MPI-1 interface. The grid is divided into structured blocks of equal numbers of points, as illustrated in Figure (1). Each block covers the entire span of the simulated section of airfoil.

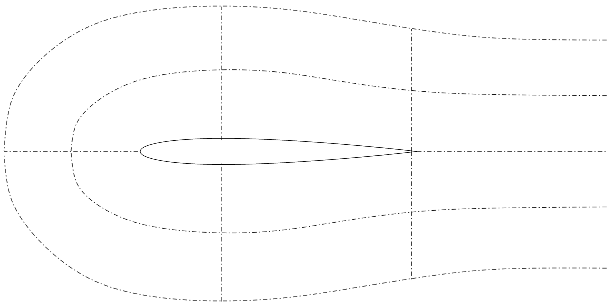

Figure 1. Decomposition of the computational domain around the NACA0012 airfoil into structured subgrids.

At every interface between adjacent blocks, an overlap of five points is used to allow the application of the centered eleven-point differencing scheme and filter right up to the interface. The communication procedure involves sending and receiving the values of the five physical variables ($\rho, \rho u, \rho v, \rho w, \rho e$) for all the grid points over a depth of 5 points from the interface. Figure (2) shows a simple 1D illustration of the transfer process, which is performed at every sub-iteration of the Runge-Kutta integration. Synchronisation of the

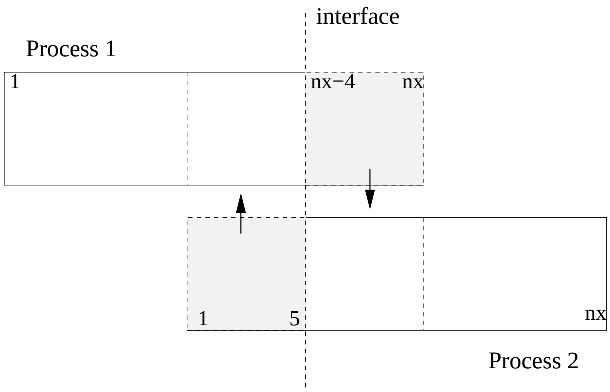

Figure 2. Illustration of the communication procedure between two subdomains composed of nx points.

communication with respect to the underlying numerical algorithm, and in particular with respect to the spatial differencing, is essential. To this end, the MPI_BARRIER routine is used to ensure that the spatial derivatives at points in the interface regions are calculated with the most up-to-date values of the variables. The parallelization of a large-stencil-size finite-difference code leads to relatively large amounts of data being transferred at each interface between neighbouring sub-domains. Indeed, for a two-dimensional interface between two sub-domains, measuring 50 by 50 points, each communication call requires the transfer of $50 \times 50 \times 5_{\text{depth}} \times 5_{\text{variables}} \times 64_{\text{double-precision bits}} \times 2_{\text{send / receive}} \approx 1$ MB of data. Fortunately, clusters now have very fast networks, typically capable of transferring at least 1Gbit/s, and dedicated cluster networks also have very short latencies, so that the actual time cost of these large data transfers remains small compared to that of the Navier-Stokes resolution. In the simulations shown in this work, the transfer time on an ethernet-based network always remained inferior to 5% of the wall-time, and substantially less on a dedicated network. Figure (3) shows the acceleration rate obtained thanks to the parallelization, on a cluster of ALPHA EV68 1250 MHz processors connected by a Hippi communications network. The same total computational domain was used for all but the single processor case, where a smaller domain was used due to memory issues. Overall, the acceleration results indicate that the parallel code scales well, at least for the moderate numbers of sub-domains so far tested. The results also show that parallelized high-order large-stencil schemes do not necessarily incur unreasonable communication overheads, and that their use for highly parallelized simulations is not proscribed.

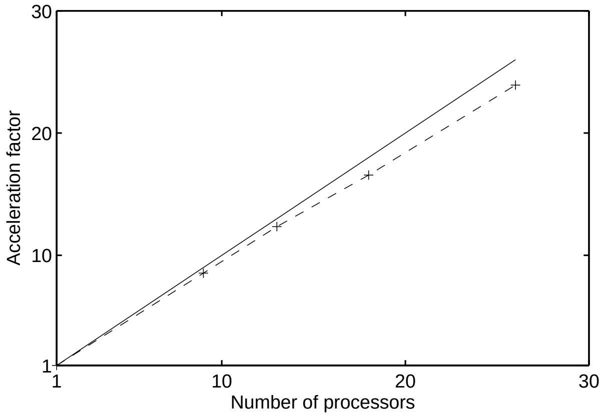

Figure 3. Speedup obtained thanks to parallelization, as a function of the number of processors. – theoretical linear acceleration, + - - + acceleration obtained

IV. Two-dimensional airfoil

Preliminary NACA0012 calculations were performed in two dimensions, to investigate the behaviour of the code around the trailing edge, as well as to provide comparison points for the three-dimensional simulations. The airfoil chord is set to $c = 0.1$m, and the incoming flow has a Mach number of M$= 0.22$. This yields a chord-based Mach number of $\mathrm{Re}_c = 500,000$. The computational grid is composed of 1400 points in the azimuthal direction and 280 points in the radial direction. Figure (4) shows the RMS velocity fluctuations, rendered non-dimensional by the free-stream velocity U_∞, in the upper and lower boundary layer. The velocity fluctuations are measured at a height of $h_y = 0.0035 \times c$ above the airfoil surface. They are equal to zero up to $x/c \approx 0.3$, indicating that the boundary layer is laminar up to this point, and their subsequent progressive increase is due to the appearance and development of the vortical structures visible in Figure (5). Transition from a laminar state thus appears to begin considerably too close to the leading-edge, as experimental data[18, 27, 28] indicate the transition zone to start between $x/c = 0.6$ and $x/c = 0.7$. Figure (5) presents a snapshot of the instantaneous vorticity field around the NACA0012 airfoil. The behaviour of the vorticity is adversely affected by the two-dimensional aspect of the simulation. Indeed, the lack of mixing of the positive and negative vorticity is noticeable, and positive/negative vortex pairs visible downstream from the airfoil have left the wake zone due to their induced velocity. Furthermore, the vorticity field appears to be composed of overly large vortices and is free of small vortical structures, which is not the case in the snapshot of a cut of the vorticity field around the three-dimensional airfoil, shown in Figure (10). In fact, despite starting to undulate early compared to experimental data, the boundary layer fails to transition to a turbulent state, due perhaps to the fact that secondary instabilities leading to turbulent boundary layers are three-dimensional in nature. An additional consequence of the abnormal vorticity development along the airfoil's surface is an increased boundary layer thickness, of the order of 4 mm at the trailing edge, to be compared with 2 mm in the three-dimensional simulation. However, the directivity of the computed pressure field agrees fairly well with the directivity obtained by Oberai *et al*[29] for the wavelength $\lambda = c/2.26$, which is the closest match to the dominant wavelength $\lambda = c/4.5$ found in our simulation.

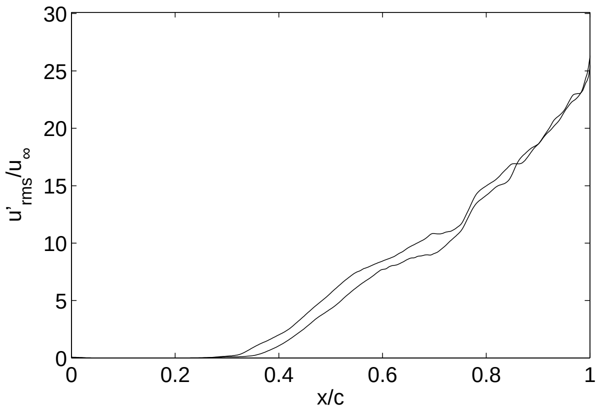

Figure 4. Turbulent velocity fluctuations u'_{rms}/U_∞ in the upper and lower boundary layers at a distance of $h_y = 0.0035 \times c$ above the airfoil surface, plotted as a function of x/c.

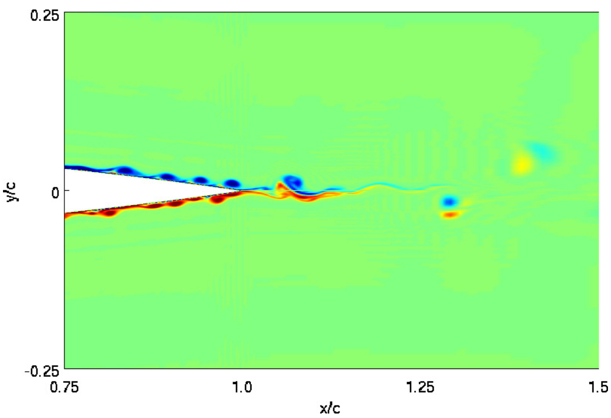

Figure 5. Vorticity intensity around a 2D NACA0012 airfoil at a chord-based Reynolds number of Re$_c = 500,000$. Color scale is between $\pm 3 \times 10^5$

V. Three-dimensional airfoil

A parallel simulation of the three-dimensional flow around a NACA0012 is now presented. The flow configuration is identical to that used in the two-dimensional simulation: the airfoil chord is $c = 0.1$m and the Mach number of the incoming flow is M$= 0.22$. The C-type grid used for the simulation is composed of 11.9×10^6 points, distributed as follows: 1200 points in the azimutal direction, 220 in the radial direction and 45 points in the spanwise direction. Grid spacings near the airfoil are identical to those used for the two-dimensional simulation. The 45 spanwise points correspond to a length of roughly 5% of the chord. This span is larger than those often used in LES of airfoils (Mary and Manoha[30] for example simulated a span corresponding to 1.5% of the chord), but the Reynolds number is lower in the present work, meaning that transversal characteristic lengths are larger. The results presented here were obtained after an initial transitory period of 140,000 iterations, corresponding to 5 convection times along the airfoil. Average quantities such as mean velocity profiles in the wake and the wake centerline velocity defect are traced in Figures (7) and (8), and

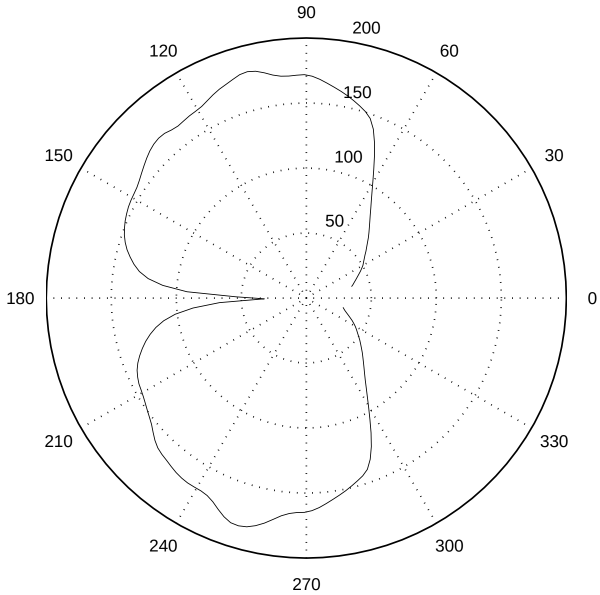

Figure 6. RMS pressure directivity around the 2D NACA0012 airfoil, measured at $r/c = 1.5$.

compared with experimental data measured by Hah and Lakshminarayana[31] in the wake of a weakly inclined NACA0012 airfoil at a chord-based Reynolds number of $\mathrm{Re}_c = 3.8 \times 10^5$.
The velocity deficit $(U_\infty - U)$ is scaled by the maximum deficit $(U_\infty - U_c)$ where U_c is the velocity on the wake centerline, and is plotted as a function of y scaled by the height l_s at which the velocity defect is halved. The profiles compare favorably with the Gaussian function $\exp[-0.7(y/ls)^2]$, as do Hah's measured data. The velocity defect profile at the trailing edge $(x/c = 1.0)$ deviates notably from the autosimilar solution, as also noted by Hah, which is not surprising since the autosimilar expression was originally derived for a far wake.[33] Likewise, the velocity recovery in the wake, over the short wake distance actually resolved in the computation, shows reasonable agreement with Hah's experimental data. The data measured by Chevray and Kovasznay[32]) in the wake of a flat plate are also included for comparison.

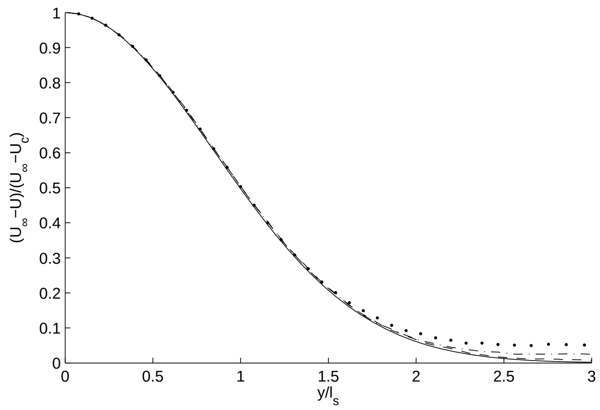

Figure 7. Mean velocity defect profiles in the wake at ········ x/c=1.0 $-\cdot-\cdot-$ x/c = 1.1 - - - x/c=1.2 — Gaussian function $\exp[-0.7(y/ls)^2]$

A mean drag coefficient of $C_d = 0.02$ is found, which is a little higher than the value of 0.011 obtained by Hah and Lakshminarayana for an airfoil at a lower Reynolds number of $380,000$ and $3°$ angle of attack. The mean pressure coefficient $C_p = (p - p_\infty)/(0.5\rho u_\infty^2)$, shown on Figure (9), corresponds very closely to that measured by Lee and Kang[18] for NACA0012 airfoils at Reynolds numbers of $400,000$ and $600,00$ and at zero degrees incidence to the mean flow.

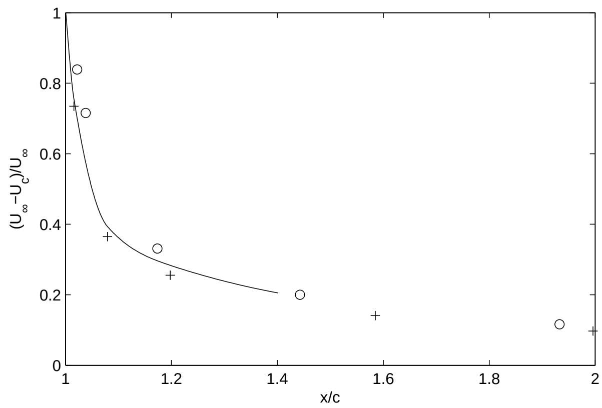

Figure 8. Decay of the wake centerline velocity defect. ○ NACA0012 airfoil at 3° incidence and $\mathrm{Re}_c = 3.8 \times 10^5$ (Hah and Lakshminarayana[31]) + flat plate wake(Chevray and Kovasznay[32]) — present simulation

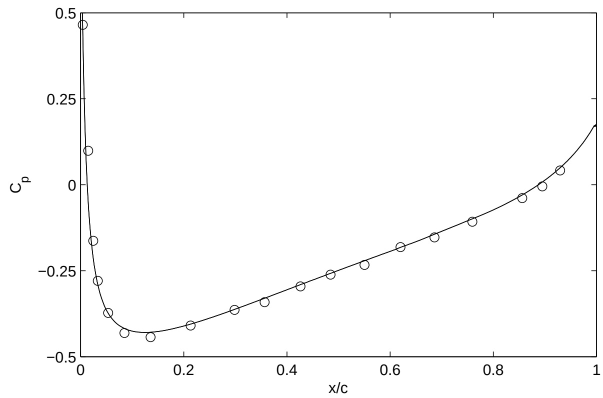

Figure 9. Mean pressure coefficient $C_p = (p - p_\infty)/(0.5\rho u_\infty^2)$ around a NACA0012 airfoil. ○ airfoil at Reynolds number of 600,000 (Lee and Kang[18]), — present simulation

According to experimental data available, the boundary layers around the airfoil transition from a laminar to a turbulent state before reaching the trailing edge. Kerho and Bragg[28] examined a NACA0012 airfoil at a Reynolds number of 7.5×10^5 and situated the beginning of the transition zone at $x/c = 0.65$, and the end of the zone -*i.e.* the beginning of the fully turbulent zone- at $x/c = 0.78$. Gartenberg and Roberts,[27] working at a lower Reynolds number of 3.75×10^5, found the boundary layer to remain laminar up to $x/c = 0.8$, while Lee and Kang[18] found the transition zone for an airfoil at a Reynolds number of 6×10^5 to be located between $x/c = 0.62$ and $x/c = 0.78$. It should be noted that the location and length of the transition zone is very dependent on experimental conditions, and in particular on the background turbulence level of the upstream flow.

Figure (10) presents an (x, y) cut of the instantaneous vorticity field $\Omega_z = \partial v/\partial x - \partial u/\partial y$ around rear half of the airfoil. The boundary layer is laminar to around $x/c = 0.6$, and from $x/c = 0.65$ onwards, the vorticity starts to undulate and progressively rolls up into vortical structures of wavelength $\lambda \approx 0.0024$ m. These structures correspond to Tollmien-Schlichting instabilities, and are characteristic sign of the beginning of transition in a boundary layer. The wavelength of $\lambda \approx 0.0024$ m is in good agreement with the value of 0.0021m predicted by linear instability theory. Figure (11) shows top and side isosurface views of the streamwise vorticity $\Omega_x = \partial w/\partial y - \partial v/\partial z$ near the trailing edge of the airfoil. The streamwise vorticity masks the initial Tollmien-Schlichting instabilities that start around $x/c = 0.65$, and highlights the secondary instabilities that develop farther downstream. At $x/c = 0.9$, strongly organized streamwise structures appear, that resemble low-speed streaks characteristic of near-wall turbulence. The spanwise distance δ_z^+ measured in wall units separating these structures is approximately $\delta_z^+ = 110$, which is very close to the value of $\delta_z^+ = 100$ typically found in the literature.[34] The end of the transition zone in the simulation is located slightly farther downstream than experimental data would tend to indicate, but it is as yet unclear whether this is due to the complete absence of turbulence in the incoming flow, a condition not easily to achieve experimentally, or to numerical aspects of the simulation.

Figure (12) presents an (x, y) cut of the instantaneous pressure field around the airfoil. It is obtained directly by the LES simulation, without the use of a separate wave equation. The radiation is strongly dipolar due to the remanents of the Tollmien-Schlichting instabilities crossing the trailing edge, with a marked upstream directivity. Calculations currently under way will allow the direct computation of a substantially larger zone of radiated field, as well as detailed analyses of the acoustic perturbations.

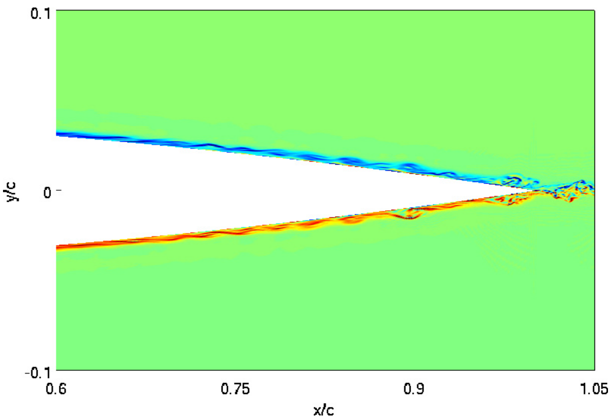

Figure 10. Instantaneous vorticity field $\Omega_z = \partial v/\partial x - \partial u/\partial y$ around a 3D NACA0012 airfoil at a chord-based Reynolds number of $\mathbf{Re}_c = 500,000$. Color scale is between $\pm 3 \times 10^5$

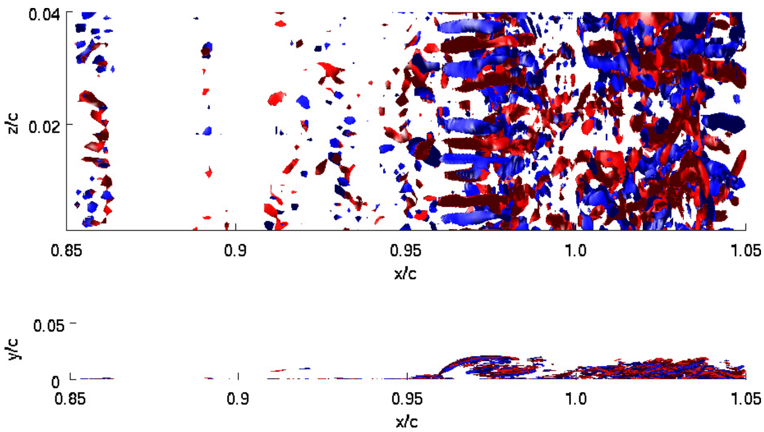

Figure 11. Streamwise vorticity in the upper boundary layer near the trailing edge. Top and side isosurface views of $\Omega_x = \partial w/\partial y - \partial v/\partial z$. Red and blue isosurfaces correspond respectively to 1.5×10^5 and -1.5×10^5. Distances are rendered nondimensional by the airfoil chord c.

VI. Conclusions

A three-dimensional parallel Large Eddy Simulation code, solving the compressible Navier-Stokes equations on structured curvilinear grids thanks to high-order explicit finite differences and filters, is presented. A NACA0012 airfoil at zero incidence and at a Reynolds number of 500,000 is then studied, both in two dimensions and in three dimensions. The flow parameters are such that the boundary layers around the airfoil are initially laminar, and transition to a turbulent state before reaching the trailing edge. Results obtained by simulating the two-dimensional Navier-Stokes equations show that the boundary layer dynamics are not correctly captured in two dimenions, but that the resulting acoustic perturbations are correctly propagated. The three-dimensional parallel code is shown to capture the transition dynamics in the boundary layers, and both mean and fluctuating flow values around the airfoil match experimental data reasonably well. More

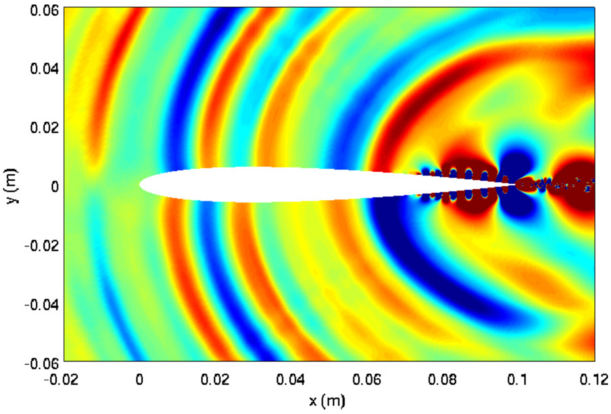

Figure 12. Instantaneous pressure fluctuations around a 3D NACA0012 airfoil at a chord-based Reynolds number of Re$_c = 500,000$. Color scale between $\pm$20Pa.

detailed analyses of the flow statistics as well as the radiated acoustic field are currently under way.

Acknowledgements

This work was undertaken with the financial support of Electricité de France, Direction Recherche & Développement under the supervision of Dr. Philippe Lafon. A part of the computations was carried out on one of the parallel supercomputers of the CEA (the French Atomic Energy Agency) in France.

References

[1]Tam, C. and Webb, J., "Dispersion-relation-preserving finite difference schemes for computational acoustics," *J. Comput. Phys.*, Vol. 107, 1993, pp. 262–281.

[2]Bogey, C. and Bailly, C., "A family of low dispersive and low dissipative explicit schemes for noise computations," *J. Comput. Phys.*, Vol. 194, No. 1, 2004, pp. 194–214.

[3]Lele, S., "Compact finite difference schemes with spectral-like resolution," *J. Comput. Phys.*, Vol. 103, 1992, pp. 16–42.

[4]Visbal, M. and Gaitonde, D., "High-order-accurate methods for complex unsteady subsonic flows," *AIAA Journal*, Vol. 37, No. 10, 1999, pp. 1231–1239.

[5]Kurbatskii, K. and Tam, C., "Cartesian boundary treatment of curved walls for high-order computational aeroacoustics schemes," *AIAA Journal*, Vol. 35, No. 1, 1997, pp. 133–140.

[6]Benek, J., Steger, J., Dougherty, F., and Buning, P., "Chimera: A Grid-Embedding Technique," *AEDC-TR-85-64*, 1986.

[7]Lummer, M., Delfs, J. W., and Lauke, T., "Simulation of sound generation by vortices passing the trailing edge of airfoils," *AIAA Paper 2002-2578*, 2002.

[8]Ffowcs Williams, J. and Hall, L., "Aerodynamic sound generation by turbulent flow in the vicinity of a scattering half-plane," *J. Fluid Mech.*, Vol. 40, 1970, pp. 657–670.

[9]Crighton, D., "Radiation from vortex filament motion near a half-plane," *J. Fluid Mech.*, Vol. 51, 1972, pp. 357–362.

[10]Howe, M., "Contributions to the theory of aerodynamic sound, with application to excess noise and the theory of the flute," *J. Fluid Mech.*, Vol. 71, 1975, pp. 625–673.

[11]Howe, M., "The influence of vortex shedding on the generation of sound by convected turbulence," *J. Fluid Mech.*, Vol. 76, No. 4, 1976, pp. 711–740.

[12]Schlinker, R., "Airfoil trailing edge noise measurements with a directional microphone," *AIAA Paper 77-1269, Atlanta, Georgia*, 1977.

[13]Yu, J. and Joshi, M., "On sound radiation from the trailing edge of an isolated airfoil in a uniform flow," *AIAA Paper 79-0603*, 1979.

[14]Brooks, T. and Hodgson, T., "Trailing Edge Noise Prediction from Measured Surface Pressures," *J. Sound Vib.*, 1981, pp. 69–117.

[15]Singer, B., Brentner, K., Lockard, D., and Lilley, G., "Simulation of acoustic scattering from a trailing edge," *J. Sound Vib.*, Vol. 230, No. 3, 2000, pp. 541–560.

[16]Wang, M. and Moin, P., "Computation of trailing-edge flow and noise using Large-eddy simulation," *AIAA Journal*, Vol. 38, No. 12, 2000, pp. 2201–2209.

[17]Manoha, E., Herrero, C., Sagaut, P., and Redonnet, S., "Numerical prediction of airfoil aerodynamic noise," *AIAA Paper 2002-2573*, 2002.

[18]Lee, H. and Kang, S., "Flow characteristics of transitional boundary layer on the NACA0012 airfoil in wakes," *Proceedings of FEDSM'98, Washington, DC*, June 21-25 1998.

[19]Berland, J., Bogey, C., and Bailly, C., "Optimized Explicit Schemes: Matching and Boundary Schemes, and 4th-order Runge-Kutta Algorithm," *AIAA Paper 2004-2814*, 2004.

[20]Visbal, M. and Gaitonde, D., "Very high-order spatially implicit schemes for computational acoustics on curvilinear meshes," *J. Comput. Acous.*, Vol. 9, No. 4, 2000, pp. 1259–1286.

[21]Bogey, C. and Bailly, C., "Three-dimensional non-reflective boundary conditions for acoustic simulations : far field formulation and validation test cases," *Acta Acustica*, Vol. 88, No. 4, 2002, pp. 463–471.

[22]Visbal, M., "Benchmark Problems - Category 2 : Multi-Geometry Scattering Problem," *Fourth Computational Aeroacoustics (CAA) Workshop on Benchmark Problems*, 2003.

[23]Marsden, O., Bailly, C., and Bogey, C., "High-order curvilinear simulations of flows around non-cartesian bodies," *J. Comput. Acous.*, 2005, to appear.

[24]Visbal, M. and Rizzetta, D., "Large-Eddy Simulation on curvilinear grids using compact differencing and filtering schemes," *ASME Journal of Fluids Engineering*, Vol. 124, No. 4, 2002.

[25]Bogey, C. and Bailly, C., "Decrease of the effective Reynolds number with eddy-viscosity subgrid-scale modeling," *AIAA Journal*, Vol. 43, No. 2, 2005, pp. 437–439.

[26]Bogey, C. and Bailly, C., "Computation of a high Reynolds number jet and its radiated noise using LES based on explicit filtering," *Computers and Fluids*, 2005, accepted, to appear.

[27]Gartenberg, E. and Roberts Jr., A., "Airfoil transition and separation studies using and infrared imaging system," *J. Aircraft*, Vol. 28, No. 4, 1991, pp. 225–230.

[28]Kerho, M. and Bragg, M., "Airfoil Boundary-Layer Development and Transition with large leading-edge roughness," *AIAA Journal*, Vol. 35, No. 1, 1997.

[29]Oberai, A., Roknaldin, F., and Hughes, T., "Computation of trailing-edge noise due to turbulent flow over an airfoil," *AIAA Journal*, Vol. 40, No. 11, 2002, pp. 2206–2216.

[30]Mary, I. and Sagaut, P., "Large eddy simulation of flow around an airfoil near stall," *AIAA Journal*, Vol. 40, No. 6, 2002, pp. 1139–1145.

[31]Hah, C. and Lakshminarayana, B., "Measurement and prediction of mean velocity and turbulence structure in the near wake of an airfoil," *J. Fluid Mech.*, Vol. 115, 1982, pp. 251–282.

[32]Chevray, R. and Kovasznay, S., "Turbulence Measurements in the Wake of a Thin Flat Plate," *AIAA Journal*, Vol. 7, No. 8, 1969, pp. 1641–1643.

[33]Schlichting, H., *Boundary Layer Theory*, McGraw-Hill, 1968.

[34]Kim, H. and Reynolds, W., "The production of turbulence near a smooth wall in a turbulent boundary layer," *J. Fluid Mech.*, Vol. 50, 1971, pp. 133–160.